Modeling the Performance of Optical Modems in the DESERT Underwater Network Simulator

Alberto Signori, Filippo Campagnaro, Michele Zorzi

Abstract—While in the past decades only low rate acoustic modems were employed for underwater wireless communication, nowadays also high rate optical modems can be used for short range communication, up to a few hundred meters. A key question is what is the expected performance of a modem in a given scenario, in order to predict the coverage range of the system in a network deployment. In the literature, many models have been proposed, but each of them is limited to simulating a particular device or a limited set of scenarios. However, in the last decade, many sea evaluations of optical communications performance in different water conditions have been performed, and many datasets published and presented to the research community. In this paper we collect a database of performance figures of optical modems, including it in the DESERT Underwater network simulator. In addition, we simulate optical communication in a real scenario, thanks to the water measurements retrieved during the ALOMEX'15 NATO cruise.

Index Terms—Underwater optical communication, network simulator, NS-Miracle, DESERT, multi-modality.

I. INTRODUCTION AND RELATED WORKS

Underwater optical communications (UWOP) are a hot topic for both the research and the manufacture areas. Indeed, UWOP pave the way to several new applications, such as underwater high-definition (HD) real-time (RT) wireless video streaming [1] to remotely control underwater vehicles, efficient data muling from sensors [2], and many others. These applications allow the creation of new scenarios that can be deployed in underwater assets for marine biology, military and oil and gas industries. The key question that arises during the design of an underwater deployment is what is the actual performance of UWOP in terms of coverage range, directionality and link stability in a real scenario. Unfortunately, the answer to this question is not trivial, as UWOP may perform very differently depending on the specific environmental conditions. In particular, UWOP are affected by water turbidity, alignment between transmitter and receiver, background light noise and water temperature. This calls for a simulation tool that models UWOP accurately and provides its communication performance given the environmental conditions of a certain location. However, performing a simulation of UWOP that matches well the actual performance of real optical modems is very challenging, as each manufacturer, as well as each research institute that developed its own modem prototype, employs a different transmitter light source and a different receiver, that cannot be modeled in the same way due to the different physical properties. For instance, in [3]

F. Campagnaro (Corresponding author, email: campagn1@dei.unipd.it), A. Signori and M. Zorzi are with the Department of Information Engineering, University of Padova, Italy.

the authors employed a set of blue light emitting diodes (LEDs) as a transmitter, and a Si-PIN photo-diode [4] as a receiver, while in [5] the receiver choice was an avalanche photodiode (APD) [6]. Instead, in [1] the authors used a prism of blue LED matrices as transmitter and a receiver based upon a photomultiplier (PMT) [7]. In [8], they used a LED-based transmitter and a Silicon Photomultipliers (SiPMs) [9] receiver. In [10], the authors employed a blue and a white LED matrices as transmitter, and a photo-sensors with human-eye wavelength sensitivity receiver. Instead, both in [11] and [12], they employed a laser transmitter and a PMT receiver.

Another challenging aspect is to predict how UWOP reacts to the surrounding light noise. Direct light noise to the modem may saturate the receiver, causing the loss of the signal. Some companies and research institutes propose a modem able to limit this effect, with a noise compensation system [1], [10], [13]. However, most of these mechanisms are patented or proprietary, and therefore it is not possible to model them with free access.

Many models for simulating UWOP have been presented in the literature. For instance, in [11] and [12] the authors propose two different Monte Carlo-based models to simulate the laser transmission; however, these models are computationally expensive, specially for emitters composed by multiple light sources, such as matrices of LEDs. In [3], they modeled UWOP by employing the Beer-Lambert's exponential law, based on the attenuation coefficient c and the distance between transmitter and receiver l. However, neither an LED nor a laser is a perfect Lambertian light source. In addition, in [14] the authors state that the parameter c should only be used in the case of a narrow collimated light beam, such as a laser diode. Instead, in the case of an uncollimated beam emitter, like an LED, c does not characterize the light propagation adequately, and should be replaced by the diffuse attenuation coefficient K_d. The optical properties of the water varies along the water column. For this reason, in [10] the authors included a database of water properties to characterize real scenarios, and modeled UWOP by integrating the Beer-Lambert's law along the water column. This database includes water temperature (T), solar irradiance (E_0), optical absorption (a) and attenuation coefficients (c) of 39 different stations at different wavelengths. These measurements have been retrieved during the ALOMEX'15 research cruise, organized by the NATO STO Centre of Marine Research and Experimentation (CMRE). We extended this approach by including a database of modem performance figures, in order to match the behavior of real transmissions, by overcoming the problem of the Beer-Lambert's law. This model has been included in the DESERT
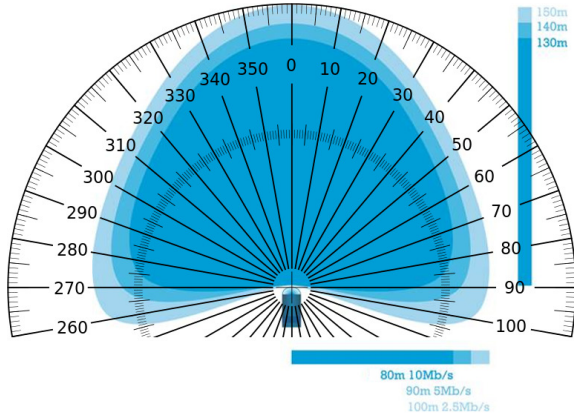
Fig. 1. BlueComm 200 operational area [17] in ideal water conditions.

Underwater simulator [15], available online [16]. In Section II, we report the implementation details of the proposed model for UWOP simulation. In Section III, we present the result obtained with our simulation approach. In Section IV we finally draw our conclusions and illustrate ongoing works.

II. IMPLEMENTATION DETAILS IN DESERT UNDERWATER

In this section we describe how the real performance of UWOP has been modeled. In Section II-A, we describe the performance lookup tables (LUTs) extrapolation, while in Section II-B we present the optical beam pattern model that has been implemented in the DESERT Underwater simulator.

A. Lookup Table Extraction

In order to include the performance figures of an optical modem in the DESERT Underwater simulator, we extrapolated a set of LUTs from the beam pattern of some state of the art transceivers. For example, the BlueComm 200 beam pattern in ideal water conditions, for different levels of bitrate, namely 2.5, 5 and 10 Mb/s, is presented in Figure 1 [17], and the Ifremer optical modem beam pattern is depicted in Figure 2 [8], when transmitting at 3 Mb/s. From this figure we extrapolated the LUT of the beam pattern section (LUT_{bp}), composed of inclination angle from the transmitter with respect to the receiver (θ) and the normalized maximum range achievable at that angle ($n_r(\theta)$). n_r has been calculated as

$$n_r(\theta_k) = R(\theta_k)/R(0), \tag{1}$$

where $R(\theta)$ is the maximum transmission range when the inclination between transmitter and receiver is $\theta = \theta_k$, and $R(0)$ is the maximum transmission range when transmitter and receiver are perfectly aligned. OPT transmitters and receivers may have a different operational area, and therefore a different LUT_{bp}. This is the case of the MIT AquaOptical prototype [5] (Figure 3). The 3D beam pattern is obtained from the rotation of the provided performance figures along the transmitter direction.

We then built the LUT of the maximum range achievable in different water conditions (LUT_{cr}) for that modem. For instance, the maximum range of the BlueComm 200 is reported in Figure 4 in the case of deep water (red line) and shallow
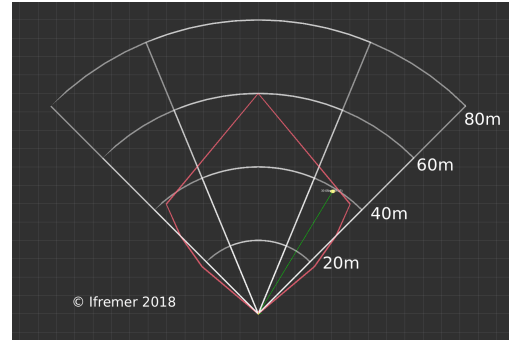

Fig. 2. Ifremer optical modem operational area when transmitting at 3 Mb/s [8] in shallow water at night, turbidity Jerlov I ($c \simeq 0.02\ m^{-1}$).
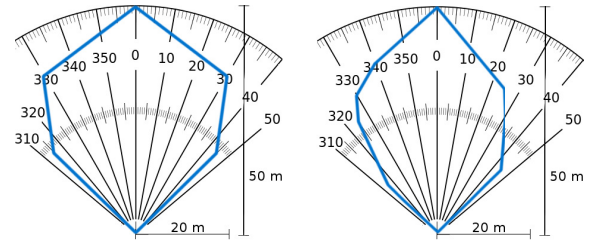

Fig. 3. The MIT AquaOptical modem operational area when the transmitter position is fixed and the receiver changes the position pointing to the transmitter (left hand side) and when the receiver is fixed and the transmitter changes the position pointing to the receiver (right hand side) as reproduced from [5]. The experiment took place in a pool, transmitting at 4 Mb/s in shallow water at night, turbidity Jerlov I ($c \simeq 0.02\ m^{-1}$).

water (blue line) scenarios, during night operations close to the coast. In the latter case, the light noise caused by moon, stars, coastal and ship lighting lowers the maximum transmission distance of UWOP. In order to create a more fine-grained LUT, we employed the MatLab Piecewise Cubic Hermite Interpolation (PCHIP) [18], that allowed us to smoothly fit the samples (Figure 4).
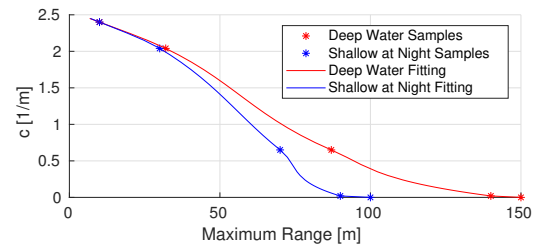

Fig. 4. BlueComm 200 maximum transmission range in different water conditions, when transmitting at 2.5 Mb/s.

B. Beam Pattern Model

Given a 3D space, we set the transmitter at the origin of the axes and we compute the inclination angles between the transmitter and the receiver. To find the maximum transmission range we compute both the inclination angle θ^{tx} between the (X-Y) plane and the straight line connecting transmitter and receiver, and the angle θ^{tx}_{XY} between the x-axis and the projection on the (X-Y) plane of the straight line connecting the transmitter and the receiver. A visualization of the inclination angles used in the model is reported in Figure 5. In general,
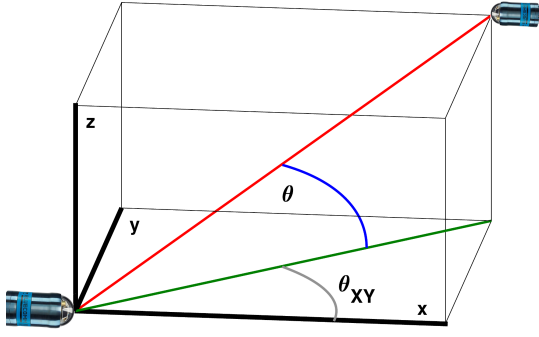
Fig. 5. Representation of the angles θ and θ_{XY}.

considering a spherical coordinate system, θ is the polar angle and θ_{XY} is the azimuthal angle. These angles have to be computed both from the transmitter's point of view and from the receiver's point of view. By default, we suppose the modem of each node to be placed in the (X-Y) plane and directed along the x-axis. We define the direction of the modem as the direction of the maximum transmission range $R(0)$, presented in Section II-A. In our model, the modem can be rotated with a rotation angle α along the (X-Z) plane. α is used to point the transmitter and receiver towards each other. Positive values of α correspond to a clockwise rotation and negative values of α to a counterclockwise rotation, i.e., with $\alpha = \pi/2$ the modem is directed toward the positive values of the z-axis and with $\alpha = -\pi/2$ rad the modem is directed toward the negative values of the z-axis, by considering the modem at the origin of the 3D space. Transmitter and receiver have their own rotation angles, α_{tx} and α_{rx} respectively.

First of all we compute the polar and the azimuthal angles from the transmitter's point of view, i.e., we compute θ^{tx} and θ^{tx}_{XY}. Given the position of the transmitter (x_{tx}, y_{tx}, z_{tx}) and the position of the receiver (x_{rx}, y_{rx}, z_{rx}), to apply our model we first compute the new coordinates of the receiver by considering the transmitter as the origin of our new 3D space:

$$\begin{aligned} \Delta_x^{rx} &= x_{rx} - x_{tx} \\ \Delta_y^{rx} &= y_{rx} - y_{tx} \\ \Delta_z^{rx} &= z_{rx} - z_{tx}. \end{aligned} \tag{2}$$

We consider the rotation angle of the transmitter equal to α_{tx}. As the first step, to compute θ^{tx} and θ^{tx}_{XY}, we perform the rotation of the axes by an angle $-\alpha_{tx}$ with respect to the y-axis. In this way the new reference system has the x-axis in the direction of the transmitter modem. The position of the receiver in the new reference system is given by

$$\begin{aligned} \tilde{\Delta}_x^{rx} &= \Delta_x^{rx} \cos(-\alpha_{tx}) - \Delta_z^{rx} \sin(-\alpha_{tx}) \\ \tilde{\Delta}_y^{rx} &= \Delta_y^{rx} \\ \tilde{\Delta}_z^{rx} &= \Delta_x^{rx} \sin(-\alpha_{tx}) + \Delta_z^{rx} \cos(-\alpha_{tx}). \end{aligned} \tag{3}$$

To compute the inclination angle θ^{tx}, first we compute

$$d_{XY}^{rx} = \sqrt{(\tilde{\Delta}_x^{rx})^2 + (\tilde{\Delta}_y^{rx})^2}, \tag{4}$$

then, if $d_{XY}^{rx} = 0$, θ^{tx} is given by

$$\theta^{tx} = \begin{cases} \pi/2 & \text{if } \tilde{\Delta}_z^{rx} > 0 \\ -\pi/2 & \text{if } \tilde{\Delta}_z^{rx} < 0 \end{cases} \tag{5}$$

Otherwise, if $d_{XY}^{rx} > 0$, θ^{tx} is given by

$$\theta^{tx} = \arctan \frac{\tilde{\Delta}_z^{rx}}{d_{XY}^{rx}}. \tag{6}$$

To compute θ_{XY}^{tx}, if $\tilde{\Delta}_x^{rx} = 0$, the inclination angle is given by

$$\theta_{XY}^{tx} = \begin{cases} \pi/2 & \text{if } \tilde{\Delta}_y^{rx} > 0 \\ -\pi/2 & \text{if } \tilde{\Delta}_y^{rx} < 0 \end{cases} \tag{7}$$

otherwise, if $\tilde{\Delta}_x^{rx} > 0$, the angle is equal to

$$\theta_{XY}^{tx} = \arctan \frac{\tilde{\Delta}_y^{rx}}{\tilde{\Delta}_x^{rx}}. \tag{8}$$

where the inverse tangent must be suitably defined to take the correct quadrant of the (X-Y) plane into account.

In a similar way, we compute the inclination angles from the receiver's point of view, i.e., θ^{rx} and θ^{rx}_{XY}. In this case we set the receiver to be at the origin of our new 3D space. We compute the inclination angle θ^{rx} between the (X-Y) plane and the straight line connecting transmitter and receiver, and the angle θ^{rx}_{XY} between the x-axis and the projection on the (X-Y) plane of the straight line connecting the transmitter and the receiver. The rotation angle of the receiver modem is α_{rx}. To set the receiver at the origin of the 3D space, the coordinates of the transmitter become

$$\begin{aligned} \Delta_x^{tx} &= x_{tx} - x_{rx} \\ \Delta_y^{tx} &= y_{tx} - y_{rx} \\ \Delta_z^{tx} &= z_{tx} - z_{rx}. \end{aligned} \tag{9}$$

Then we perform a rotation of the axes with respect to the y-axis by an angle $-\alpha_{rx}$. The coordinates of the transmitter in the new reference system become

$$\begin{aligned} \tilde{\Delta}_x^{tx} &= \Delta_x^{tx} \cos(-\alpha_{rx}) - \Delta_z^{tx} \sin(-\alpha_{rx}) \\ \tilde{\Delta}_y^{tx} &= \Delta_y^{tx} \\ \tilde{\Delta}_z^{tx} &= \Delta_x^{tx} \sin(-\alpha_{rx}) + \Delta_z^{tx} \cos(-\alpha_{rx}). \end{aligned} \tag{10}$$

Using these coordinates, the way to compute θ^{rx} and θ^{rx}_{XY} is the same employed for the transmitter. From the LUT_{bp} of the transmitter and the LUT_{bp} of the receiver, we obtain the normalized attenuation coefficients $n_r^{tx}(\theta^{tx})$, $n_r^{tx}(\theta^{tx}_{XY})$, $n_r^{rx}(\theta^{rx})$, $n_r^{rx}(\theta^{rx}_{XY})$. If the angle obtained with the previous computations is not an entry of the LUT_{bp}, a linear interpolation is performed to find the actual attenuation coefficient.

The last step is to find the maximum transmission range for the given water conditions. If transmitter and receiver are at the same depth d, we retrieve the value of c in the LUT related to this depth. If the actual value of d is not an entry of the LUT, a linear interpolation is performed. If the transmitter and the receiver are at different depths, we compute the equivalent value of the attenuation coefficient (c_{eq}), and

find the maximum transmission range for c_{eq}. Given d_N and c_N the depth and the attenuation coefficient of the deeper node and d_1 and c_1 the values related to the other node, c_{eq} is computed as the weighted average of c, using as weights the depth between 2 values of c in the LUT:

$$c_{eq} = \frac{1}{d_N - d_1} \sum_{k=1}^{N-1} \frac{c_k + c_{k+1}}{2}(d_{k+1} - d_k). \quad (11)$$

If the maximum transmission range for the given c_{eq} is $R(0)$, the actual transmission range considering the relative position of the transmitter and receiver is

$$R = R(0) \cdot n_r^{tx}(\theta^{tx}) \cdot n_r^{tx}(\theta_{XY}^{tx}) \cdot n_r^{rx}(\theta^{rx}) \cdot n_r^{rx}(\theta_{XY}^{rx}). \quad (12)$$

III. RESULTING BEAM PATTERN IN REAL SCENARIOS

In this section we present the results for the maximum transmission range of the Bluecomm 200 simulated in a real scenario. In this case we suppose that LUT_{bp} is the same for the transmitter and the receiver. For each scenario, we placed the transmitter in a static position, with the rotation angle $\alpha_{tx} = 0$ rad, and moved the receiver in different positions to find the maximum transmission range in which receiver and transmitter still communicate. In all the positions, the receiver has a rotation angle $\alpha_{rx} = \pi$ rad. We used the values of the attenuation coefficient c and noise measured during the ALOMEX'15 research cruise in 2 different locations. For each location, the average value of the attenuation coefficient $\bar{c}$ has been calculated along the water column, using Equation (11) with $d_1 = 1$ m and d_N equal to the maximum depth of the water column. The resulting beam pattern has been computed in four cases:

1) case 1: variable attenuation coefficient for different depths in the presence of surrounding light noise during a night operation;
2) case 2: variable attenuation coefficient for different depths in deep dark water;
3) case 3: $c = \bar{c}$, in the presence of surrounding light noise during a night operation;
4) case 4: $c = \bar{c}$, in deep dark water.

The first location has latitude $30°42.52'$ N and longitude $10°18.68'$ W, offshore the coast of Morocco. In this scenario the water column depth is 128 m and the transmitter is placed at a depth of 60.5 m. In Figure 6, right hand side, both the values of the attenuation coefficient for each depth (solid blue line) and the values of c_{eq} (dashed red line) computed from the transmitter point of view are depicted. In this location $\bar{c} = 0.168$ m^{-1}, and the maximum transmission range is reported in Figure 6. We can observe that in both case 3 (dotted red line) and case 4 (dotted blue line), the maximum transmission range is symmetric with respect to the transmitter depth. In cases 1 (dark green region) and 2 (turquoise region), instead, for depth bigger than the transmitter depth, the transmission range is wider than in cases 3 and 4, because the values of c_{eq} are smaller than $\bar{c}$. On the contrary, for a depth lower than the depth of the transmitter, the transmission range
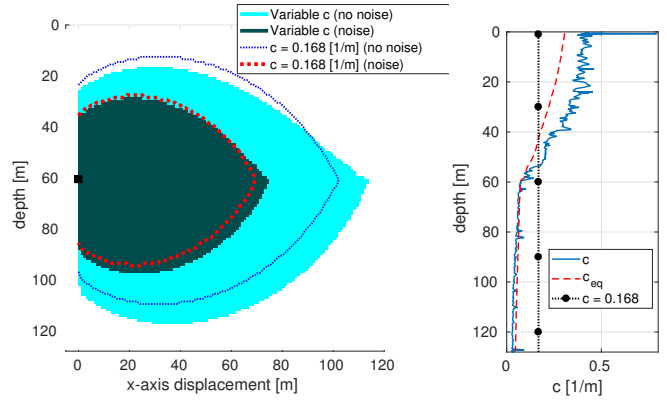

Fig. 6. Maximum transmission range in a water column of 128 m, left hand side, and the corresponding values of the attenuation coefficient and c_{eq}, right hand side.
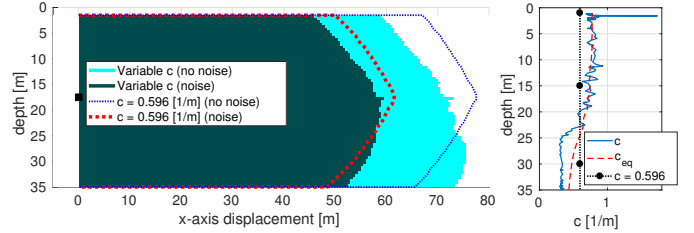

Fig. 7. Maximum transmission range in a water column of 35 m, left hand side, and the corresponding values of the attenuation coefficient and c_{eq}, right hand side

is smaller with respect to cases 3 and 4, as c_{eq} is greater than $\bar{c}$.

The second location has latitude $23°50.41'$ N and longitude $16°09.86'$ W, offshore the coast of Western Sahara. In this location the water column is 35 m deep and the transmitter is placed at a depth of 17.5 m. In Figure 7, right hand side, both the actual values of c for each depth (solid blue line) and the values of c_{eq} computed from the transmitter point of view (dashed red line) are presented, and $\bar{c} = 0.596$ m^{-1}. The maximum transmission range has been computed in the 4 cases and is reported in Figure 7, left hand side. Similarly to the previous case, the transmission range becomes bigger at increased depth, following the trend of the attenuation coefficient. In this scenario, the maximum transmission range along the x-axis is lower than in the first location, because the attenuation coefficient in this area is bigger than in the previous one, due to the high turbidity of the water.

IV. CONCLUSIONS AND FUTURE WORK

In this paper, we presented a new approach for the simulation of UWOP. Instead of employing an analytical or a Monte Carlo based model, we built a database of modem performance, retrieved from data presented in the literature. This model has been integrated with a large set of water scenario characterizations, obtained from real field measurements. Future work will include the extension of the performance figures database to a wider set of optical modems, by collecting information about both commercial modems, such as [13], [19], [20], and research prototypes, such as [5], [21], [22].

REFERENCES

[1] "Sonardyne BlueComm Optical Modem," Accessed: June. 2018. [Online]. Available: http://www.sonardyne.com/products/all-products/instruments/1148-bluecomm-underwater-optical-modem.html

[2] F. Campagnaro, F. Favaro, F. Guerra, V. Sanjuan, M. Zorzi, and P. Casari, "Simulation of multimodal optical and acoustic communications in underwater networks," in *Proc. MTS/IEEE OCEANS*, Genova, Italy, May 2015.

[3] Davide Aguita, Davide Brizzolara, Qilng Hu, "Optical Wireless Underwater Communication for AUV: Preliminary Simulation and Experimental Results," in *IEEE Oceans 2011*, 6-9 June 2011, pp. 1–5.

[4] "Si PIN photodiode S5971," accessed: June 2018. [Online]. Available: http://www.hamamatsu.com/eu/en/product/category/3100/4001/4103/S5971/index.html

[5] M. Doniec, A. Xu, and D. Rus, "Robust real-time underwater digital video streaming using optical communication," in *Proc. ICRA*, Karlsruhe, Germany, May 2013.

[6] "Cooled Large Area 5mm Blue Enhanced Silicon APD Module SD 192-70-74-661," Last time accessed: June 2018. [Online]. Available: http://datasheet.octopart.com/SD197-70-74-661-Advanced-Photonix-datasheet-146440.pdf

[7] "Photomultiplier tubes - basics and applications," accessed: June 2018. [Online]. Available: https://www.hamamatsu.com/resources/pdf/etd/PMT_handbook_v3aE.pdf

[8] P. Leon, F. Roland, L. Brignone, J. Opderbecke, J. Greer, M. Khalighi, T. Hamza, S. Bourennane, and M. Bigand, "A New Underwater Optical Modem based on Highly Sensitive Silicon Photomultipliers," in *Proc. MTS/IEEE OCEANS*, Aberdeen, UK, Oct. 2017.

[9] "A technical guide to silicon photomultipliers (SiPM)," accessed: June 2018. [Online]. Available: https://www.hamamatsu.com/us/en/community/optical_sensors/articles/technical_guide_to_silicon_photomultipliers_sipm/index.html

[10] F. Campagnaro, M. Calore, P. Casari, V. S. Calzado, G. Cupertino, C. Moriconi, and M. Zorzi, "Measurement-based Simulation of Underwater Optical Networks," in *Proc. MTS/IEEE OCEANS*, Aberdeen, UK, Oct. 2017.

[11] B. Cochenour, A. Laux, and L. Mullen, "Temporal dispersion in underwater laser communication links: Closing the loop between model and experiment," in *Proc. UCOMMS*, Lerici, Italy, Sep. 2016.

[12] F. R. Dalgleish, J. J. Shirron, D. Rashkin, T. E. Giddings, A. K. V. Dalgleish, I. Cardei, B. Ouyang, F. M. Caimi, and M. Cardei, "Physical layer simulator for undersea free-space laser communications," *Optical Engineering*, vol. 53, no. 5, pp. 1–14, May 2014.

[13] "AQUAmodem Op1 Optical Modem page," Accessed: June. 2018. [Online]. Available: {http://www.aquatecgroup.com/aquamodem/aquamodem-op1}

[14] M.-A. Khalighi, T. Hamza, S. Bourennane, P. Lon, and J. Opderbecke, "Underwater Wireless Optical Communications Using Silicon Photo-Multipliers," *IEEE Photonics Journal*, vol. 9, no. 4, pp. 1–14, Aug. 2017.

[15] P. Casari, C. Tapparello, F. Guerra, F. Favaro, I. Calabrese, G. Toso, S. Azad, R. Masiero, and M. Zorzi, "Open-source suites for the underwater networking community: WOSS and DESERT Underwater," *IEEE Network, special issue on "Open Source for Networking: Development and Experimentation"*, vol. 28, no. 5, pp. 38–46, Sep. 2014.

[16] "DESERT Underwater github repository," Last time accessed: June 2018. [Online]. Available: https://github.com/uwsignet/DESERT_Underwater

[17] "BlueComm - What's what?" Last time accessed: June 2018. [Online]. Available: https://www.sonardyne.com/bluecomm-whats-what/

[18] "Piecewise cubic hermite interpolating polynomial (pchip)," accessed: June 2018. [Online]. Available: https://it.mathworks.com/help/matlab/ref/pchip.html

[19] "Neptune underwater optical communications," accessed: June 2018. [Online]. Available: http://www.saphotonics.com/high-bandwidth-optical-communications/underwater/

[20] "About Penguin Automated Systems," accessed: June 2018. [Online]. Available: http://www.penguinasi.com/

[21] A. Caiti, E. Ciaramella, G. Conte, G. Cossu, D. Costa, S. Grechi, R. Nuti, D. Scaradozzi, and A. Sturniolo, "Optocomm: introducing a new optical underwater wireless communication modem," in *Proc. UCOMMS*, Lerici, Italy, Sep. 2016.

[22] P. Gois, N. Sreekantaswamy, N. Basavaraju, M. Rufino, L. S. J. Botelho, J. Gomes, and A. Pascoal, "Development and validation of Blue Ray, an optical modem for the MEDUSA class AUVs," in *Proc. UCOMMS*, Lerici, Italy, Sep. 2016.